



Fe³⁺ doped TiO₂ nanotubes for combined adsorption–sonocatalytic degradation of real textile wastewater

Yean Ling Pang, Ahmad Zuhairi Abdullah*

School of Chemical Engineering, Universiti Sains Malaysia, Nibong Tebal, 14300 Penang, Malaysia

ARTICLE INFO

Article history:

Received 25 July 2012

Received in revised form

14 September 2012

Accepted 28 September 2012

Available online 8 October 2012

Keywords:

Combined adsorption–sonocatalysis

Fe-doped TiO₂ nanotubes

Characteristics

Catalytic activity

Real textile wastewater

ABSTRACT

Fe-doped titanium dioxide (TiO₂) nanotubes catalyst with large specific surface area and low band gap energy were successfully synthesized using sol–gel followed by hydrothermal method. The activity of the catalyst was assessed by examining the treatment of real textile wastewater through combined adsorption and heterogeneous sonocatalysis. Fe-doped TiO₂ nanotubes exhibited better removal efficiency in the case of pre-adsorption followed by sonocatalytic reaction as compared to the simultaneous adsorption and sonocatalysis system. Pre-adsorption on TiO₂ nanotubes was found to promote sonocatalytic degradation and the latter process could be considered as a surface-catalyzed reaction. Effect of the solution pH (3–11), catalyst dosage (2–10 g/L) and hydrogen peroxide (H₂O₂) dosage (20–80 mM) on the adsorption–sonocatalysis for the treatment of a real textile wastewater were investigated in detail. The best degradation efficiency can be achieved at solution pH of 3, 6 g/L of Fe-doping, 40 mM of H₂O₂, an ultrasonic frequency of 35 kHz and an output power of 50 W after 1 h of adsorption followed by 3 h of ultrasonic irradiation under continuous aeration. The color, COD and TOC removals were 79.9%, 59.4% and 49.8%, respectively. In short, adsorption followed by sonocatalytic degradation in the presence of Fe-doped TiO₂ nanotubes showed great potential for efficient treatment of real textile wastewater.

© 2012 Elsevier B.V. All rights reserved.

1. Introduction

Textile wastewater is well-known with its high variable in composition with intense color, fluctuating pH values, high chemical oxygen demand (COD) and relatively low biodegradability with large amount of suspended solids and dissolved salts [1]. These effluents deteriorate the aesthetics of receiving water and pose significant threat to the surrounding ecosystem and human health [2]. Textile industry wastewater is usually treated using conventional physical methods such as adsorption or biological technologies [3,4]. Sludge formation and large number of aromatic rings present in organic dye compounds may cause conventional biological treatments to be ineffective for their mineralization. Moreover, adsorption may be effective for decolorization but the process only involves a phase transfer of pollutants which subsequently requires additional treatment or disposal.

Among different advanced oxidation processes, sonocatalytic degradation has received increasing attention as it possesses the potential and feasibility to remediate textile wastewater either alone or used as a pre- or post-biological treatment method [5–7]. Acoustic cavitation effect from ultrasonic irradiation causes the

formation, growth and collapse of microbubbles, which leads to the phenomenon of sonoluminescence and ‘hot spot’ with extremely high local temperature and pressure [8]. Subsequently, water molecules are dissociated to produce a large amount of free and highly reactive radicals that will directly attack the dye molecules.

Most of the research works in the field of sonocatalysis are focused on the use of TiO₂-based sonocatalysts [9,10] and other sonocatalysts such as ZnO [11] and CuO [12] for the purification of organic dyes in aqueous solution. In a previous work [13], we reported that TiO₂ nanotubes with large specific surface area, high catalytic activity and sedimentation rate showed high degradation efficiency under ultrasonic irradiation condition. However, TiO₂ nanotubes possess a relatively large band gap (~3.5 eV) [14]. One possible solution is by introducing suitable transition metals such as Fe, Cr or Co into the TiO₂-based sonocatalyst to narrow the band gap and increase the lifetime of charge carriers to promote higher catalytic efficiency [9,15,16].

Currently, most of the research works done are limited to the removal of specific dyes from pure dye solutions [1,15,17]. Information on the sonocatalytic treatment for real textile wastewater is quite scarce. Therefore, the main objective of this study is to analyze the feasibility of oxidative decolorization of textile wastewater through adsorption and ultrasonic irradiation in the presence of Fe-doped TiO₂ nanotubes. To our best of knowledge, observations on the difference between the use of pre-adsorption step followed

* Corresponding author. Tel.: +60 4 599 6411; fax: +60 4 594 1013.

E-mail address: chzuhairi@eng.usm.my (A.Z. Abdullah).

by sonocatalysis versus simultaneous adsorption–reactions have not been reported. Effects of different operating parameters on the degradation efficiency have been elucidated and the experimental results reported could offer much information on practicality of this method to treat the wastewater.

2. Experimental

2.1. Textile wastewater source and wastewater characterization

Textile wastewater without receiving any treatment was collected from a fabric textile factory located in Penang, Malaysia. The main waste streams from the dyeing, printing and finishing operations are combined in an equalization tank from which the sample was taken. The real textile wastewater contained a mixture of organic dyes which included reactive, vat and disperse dyes. The main products of this industry is dyed and printed polyester/cotton blended woven fabric with a production rate of about 10 million yards per month and produces about 250 m³/h of wastewater. The pH, color, COD and TOC of original textile wastewater were about 12, 1080 Pt/Co, 1600 mg/L and 522 mg/LC, respectively.

2.2. Preparation of TiO₂ nanotubes and Fe-doped nanotubes

Hydrochloric acid (HCl, 37%), sodium hydroxide (NaOH, 99%), tetra-*n*-butyl-orthotitanate (C₁₆H₃₆O₄Ti or Ti(OBu)₄ for synthesis, ≥98%), ethanol (CH₃CH₂OH, 96%) hydrogen peroxide solution (H₂O₂, 30%, w/w) and iron (III) nitrate nanohydrate (Fe(NO₃)₃·9H₂O, ≥98%), were obtained from Merck. Sulfuric acid (H₂SO₄, 95–97%) was purchased from Fluka Chemie Company. All the chemical reagents were used as received.

Firstly, TiO₂ powder was synthesized using a sol–gel process and calcined at 500 °C for 3 h before being used to prepare un-doped and Fe-doped TiO₂ nanotubes. The detailed procedures for preparing the TiO₂ powder and un-doped TiO₂ nanotubes catalysts have been reported earlier [13]. A hydrothermal method to prepare Cr-doped TiO₂ nanotubes as reported by Tsai and Teng [18] was followed to prepare the Fe-doped TiO₂ nanotubes. An appropriate amount of Fe(NO₃)₃·9H₂O was added to a mixture of TiO₂ powder and NaOH for hydrothermal treatment. The molar ratio of Fe to Ti prepared was 0.005. The resulting powder was finally calcined at 300 °C for 2 h to get the un-doped and Fe-doped TiO₂ nanotubes. It should be noted that a preliminary experiment was carried out and Fe-doped TiO₂ nanotubes at Fe:Ti ratio of 0.005 mol had the highest apparent first-order kinetic constant [19]. Therefore, this catalyst was chosen as the desired catalyst to be used in this study.

2.3. Sample characterizations

The structure and morphology of the un-doped and Fe-doped TiO₂ nanotubes at Fe:Ti=0.005 were analyzed using a Phillips CM 12 transmission electron microscope (TEM) which was operated at 120 kV. Raman spectroscopy analyses were performed using a Horiba Jobin Yvon HR800UV spectrometer. The diffuse reflectance spectroscopy (DRS) analyses were obtained using a UV-vis scanning spectrophotometer (PerkinElmer Lambda 35) in the wavelength range of 200–800 nm. The specific surface area and pore size measurements were determined using a surface analyzer (Quantachrome USA Autosorb -1 CLP). The content of Fe in Fe-doped TiO₂ nanotubes was determined using an atomic absorption flame emission spectroscope (AAS) (Shimadzu AA-6650). In this measurement, a known weight of powdered sample was dissolved in hot concentrated sulfuric acid solution and then diluted to known volume and used as a solution for estimation of Fe content [20].

Thermogravimetric-differential thermal analyses (TGA–DTA) were performed using a PerkinElmer STA 6000 operated at a

heating rate of 10 °C/min and in the presence of air flow rate of 20 ml/min. The zeta potential of the TiO₂ powder, un-doped and Fe-doped TiO₂ nanotubes under several pH values were measured using a zetasizer nano ZS ZEN 3600 apparatus (Malvern Instruments, United Kingdom). In order to study the surface charges of catalysts in suspension, 0.05 g of TiO₂ sample was dispersed in 1 L of 0.001 M NaCl solutions and the solution pH was adjusted by adding either 0.1 M HCl or 0.1 M NaOH.

2.4. Adsorption–sonocatalytic degradation of real textile wastewater and analysis of liquid samples

In a typical process, 6 g/L of catalyst was added into 200 mL of the real textile wastewater. Afterwards, the suspension was stirred for 1 h to reach an adsorption equilibrium. Then, the suspension was placed in an ultrasonic bath (Elma Transsonic series Ti-H5) at an operated ultrasonic frequency of 35 kHz and an output power of 50 W. During adsorption and sonocatalytic reactions, 5 mL of liquid sample was taken out at a suitable time interval and centrifuged at 4000 rpm to separate the catalyst.

COD and TOC determination were conducted using commercially available test kits provided by Hach Company. TOC was determined by removing inorganic carbon under acidic conditions, while organic carbon was digested by sodium persulfate and sulfuric acid to form carbon dioxide (CO₂) within the range of 20–700 mg/L carbon. During the digestion, CO₂ diffused into the inner ampule, which contained a pH indicator to form carbonic acid. The extent of color change at blue pH indicator correlates with the amount of carbonic acid formation, which was proportional to the total amount of carbon that presented in the sample. After the digestion process, the COD and TOC levels were measured by means of a colorimeter (Hach DR/890). The true color was analyzed using a DR/890 colorimeter according to the recommended procedure [21]. To study the extent of Fe-leaching from the catalyst, the supernatant at the end of the experiment was collected to determine the dissolved Fe concentration using AAS.

3. Results and discussion

3.1. Characterization of TiO₂ powder, un-doped and Fe-doped TiO₂ nanotubes catalysts

A transmission electron microscope was used to characterize the surface morphology of the TiO₂ powder, TiO₂ nanotubes and Fe-doped TiO₂ nanotubes. Fig. 1(a) shows that the TiO₂ particles had dimensions of about 15–25 nm. Fig. 1(b) and (c) shows that the samples are almost made up of nanotubes with diameters of approximately 10 nm with hollow structure and open ended. Their lengths ranged from several hundred nanometers to several micrometers.

The Raman spectra of TiO₂ powder, TiO₂ nanotubes and Fe-doped TiO₂ nanotubes are shown in Fig. 2. TiO₂ powder showed a typical characteristic of anatase TiO₂ at peaks around 145, 195, 399, 519 and 638 cm⁻¹ [22,23]. The absence of the most intensive anatase peak at 145 cm⁻¹ suggested the formation of trititanate (H₂Ti₃O₇) nanotubes from TiO₂ powder. Bavykin et al. [22] reported that the transformation of H₂Ti₃O₇ to intermediate phases of H₂Ti₆O₁₃, H₂Ti₁₂O₂₅ and anatase phase might occur after calcination at temperatures above 250 °C. Thereby, both nanotubes catalysts show characteristic anatase peaks at around 399, 519 and 638 cm⁻¹. A relatively higher intensity and no obvious effect of dopant on the vibrational modes of anatase phase could be observed after Fe-doped on TiO₂ nanotubes. This observation confirmed that Fe³⁺ could have occupied the substitutional sites in TiO₂ nanotubes lattice. The presence of iron was detected through AAS

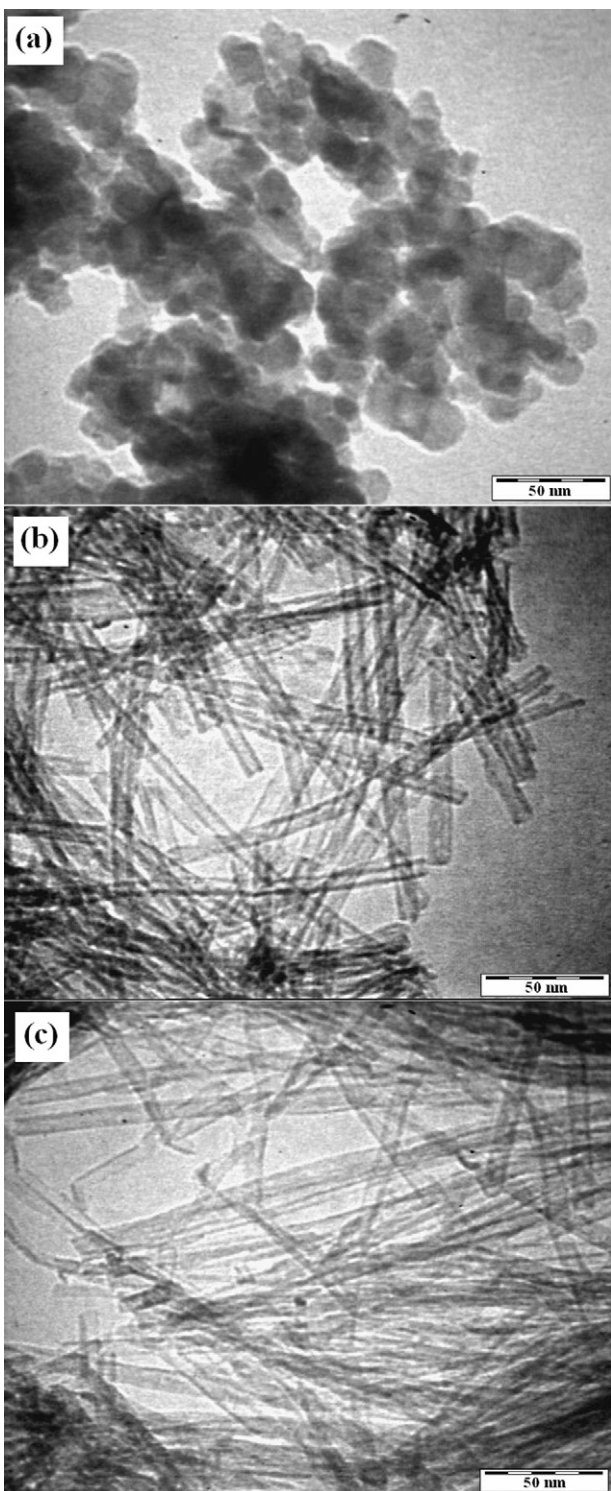


Fig. 1. TEM images of (a) TiO_2 powder (b) TiO_2 nanotubes and (c) Fe-doped TiO_2 nanotubes.

analysis and the detected mole fraction of Fe was about 0.4964 which corresponded to 100 moles of Ti.

Fig. 3(a) shows the TGA curves of the TiO_2 powder, TiO_2 nanotubes and Fe-doped TiO_2 nanotubes. The weight loss in the temperature range from 27 to 100 °C for all these catalysts was associated with the desorption of physically absorbed water or residual solvents during sol–gel process. Correspondingly, an endothermic peak below 100 °C from the DTA curves can be seen in Fig. 3(b). Meanwhile, the weight loss (7.43%) at a region between

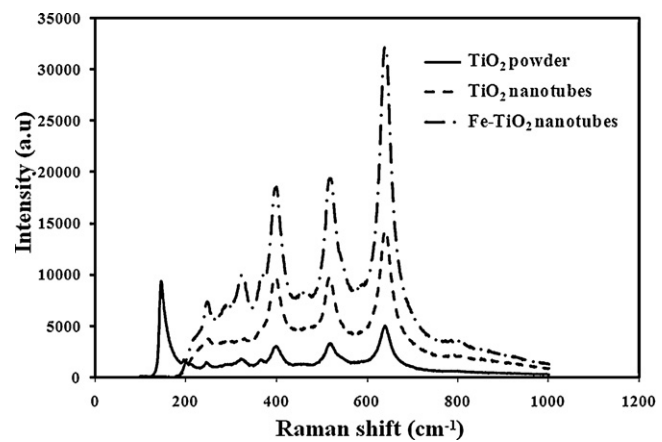


Fig. 2. Raman spectra of TiO_2 powder, TiO_2 nanotubes and Fe-doped TiO_2 nanotubes.

100 and 500 °C of the TiO_2 powder can be attributed to the removal of chemisorbed water from the TiO_2 and the decomposition of trace absorbed organic residues that were trapped inside the pores [14]. The total weight loss from 100 to 500 °C of the TiO_2 nanotubes and Fe-doped TiO_2 nanotubes were 7.96 and 8.03%, respectively as shown in Table 1. Morgado et al. [24] tried to calculate the formula of the trititanates ($\text{H}_2\text{Ti}_3\text{O}_7$) from the thermogravimetric measurements. The thermal decomposition of $\text{H}_2\text{Ti}_3\text{O}_7$ ($\text{H}_2\text{Ti}_3\text{O}_7 \rightarrow 3\text{TiO}_2 + \text{H}_2\text{O}$) showed about 7–9% of weight

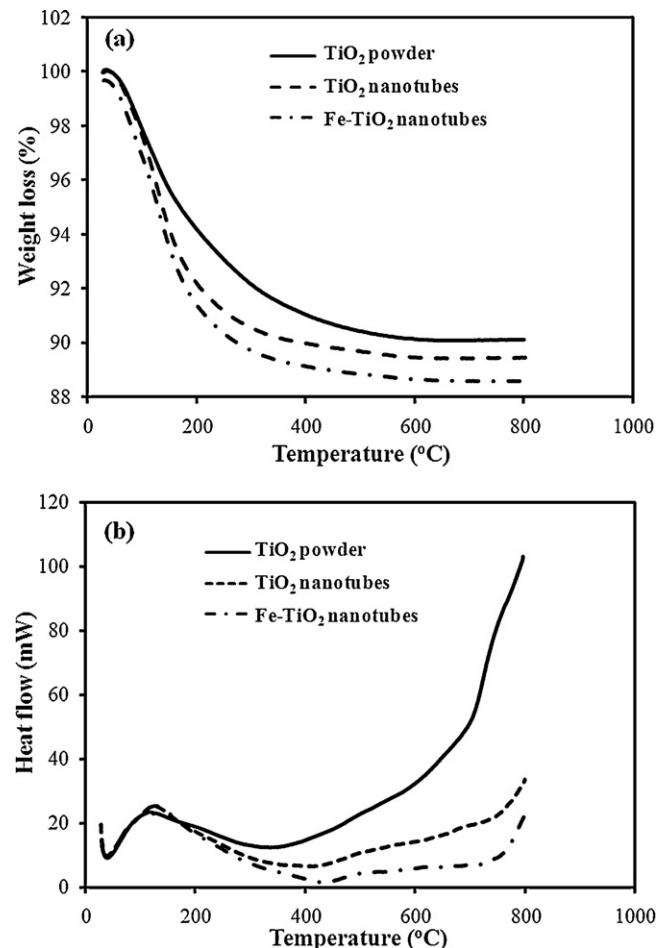


Fig. 3. (a) Thermogravimetric and (b) differential thermal analysis curves of TiO_2 powder, TiO_2 nanotubes and Fe-doped TiO_2 nanotubes.

Table 1

Weight losses (%) of TiO_2 powder, TiO_2 nanotubes and Fe-doped TiO_2 nanotubes at different temperature ranges as determined using TGA under air flow.

Temperature (°C)	27–100	100–200	200–500	100–500	500–800
TiO_2 powder	2.13	3.68	3.75	7.43	0.3
TiO_2 nanotubes	2.35	5.45	2.51	7.96	0.21
Fe-doped TiO_2 nanotubes	3.15	5.48	2.54	8.03	0.25

loss between 100 and 500 °C. This was attributed to the chemically bound H_2O in its stoichiometry apart from the structural hydroxyl ($-\text{OH}$).

Fe-doped TiO_2 nanotubes show the largest endothermic peak at around 437 °C was due to the dehydration of interlayered water (H_2O), intralayered $-\text{OH}$ groups and decomposition of organic compounds such as nitrite ions [15,24]. The heat evolved started to accelerate at 720 °C to achieve another exothermic peak at higher temperature which indicated the phase transformation from anatase to rutile phase. Besides, the weight loss between 500 and 700 °C was attributed to the oxidation of residual carbon and evaporation of chemisorbed water.

Fig. 4(a) shows the diffuse reflectance spectra of TiO_2 powder, TiO_2 nanotubes and Fe-doped TiO_2 nanotubes. It was obvious that the absorbance of Fe-doped TiO_2 nanotubes increased as compared to the un-doped TiO_2 nanotubes. This is attributed to the electron transfer transition from the valence band to dopant level or

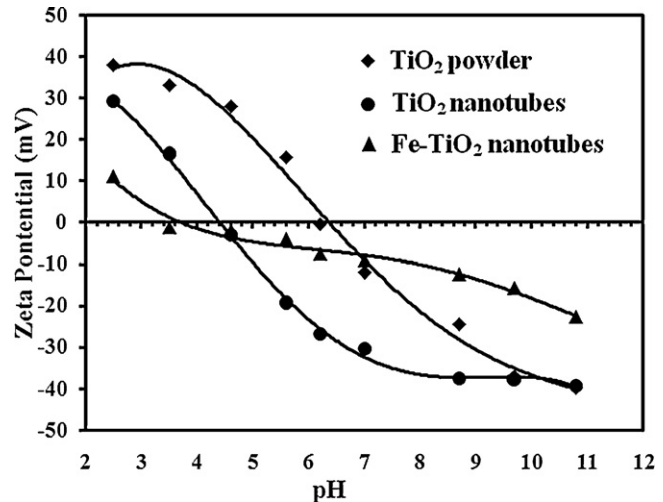


Fig. 5. Zeta potential as a function of pH for different catalyst suspensions.

from dopant level to conduction band, leading to lower band gap energy as compared to the un-doped TiO_2 nanotubes. By using Tauc's relationship [19], the indirect band gap energies for TiO_2 powder, TiO_2 nanotubes and Fe-doped TiO_2 nanotubes were calculated to be 2.91 eV, 3.11 eV and 2.70 eV, respectively (Fig. 4(b)). The band gap energy of TiO_2 nanotubes was larger than that of TiO_2 powder. This blue shift was due to the quantum size effect on different morphology of catalysts as reported by other researchers [25].

BET surface area for TiO_2 powder, TiO_2 nanotubes and Fe-doped TiO_2 nanotubes were $77.0 \text{ m}^2/\text{g}$, $155.4 \text{ m}^2/\text{g}$ and $167.6 \text{ m}^2/\text{g}$, respectively. According to the IUPAC classification, their respective pore sizes of 94.27 \AA , 56.1 \AA and 67.6 \AA are within the mesopore size range. It is predicted that the inner and outer surfaces of layered-tubular structure are the major reason for the increase in surface area, which was one of the new attribute of this nanocatalyst compared with the starting material. Other characterizations on un-doped and Fe-doped TiO_2 nanotubes such as XRD patterns and XPS had been discussed in our recently published work [19].

The measured zeta potentials as a function of pH for TiO_2 powder, TiO_2 nanotubes and Fe-doped TiO_2 nanotubes suspensions are shown in Fig. 5. The zero point charge (zpc) of TiO_2 powder, TiO_2 nanotubes and Fe-doped TiO_2 nanotubes were at pH values of around 6.4, 4.6 and 3.6, respectively. The variation of pH_{zpc} between these catalysts is due to the change in crystal structure and charge imbalance created due to substitution of Ti^{4+} atoms by Fe^{3+} in the TiO_2 structure [26]. The lower pH_{zpc} means more hydroxyl groups existing on the surface of catalyst and these groups would react with hole (h^+) to produce hydroxyl radicals ($\cdot\text{OH}$) which are strong oxidizing agents [27]. According to the following chemical equations, the surface of TiO_2 will be positively charged at pH below pH_{zpc} , whereas negatively charged at pH above pH_{zpc} and neutral at pH_{zpc} .

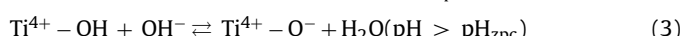
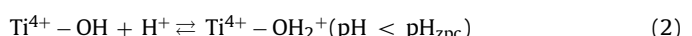
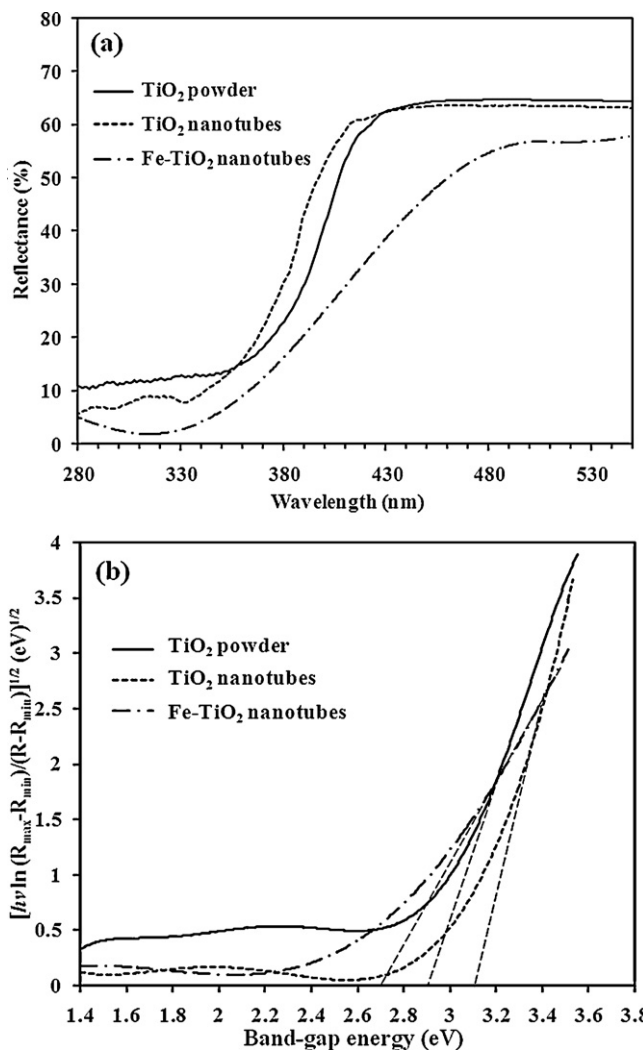


Fig. 4. (a) UV-vis diffuse reflectance spectra and (b) band gap energies of TiO_2 powder, TiO_2 nanotubes and Fe-doped TiO_2 nanotubes.



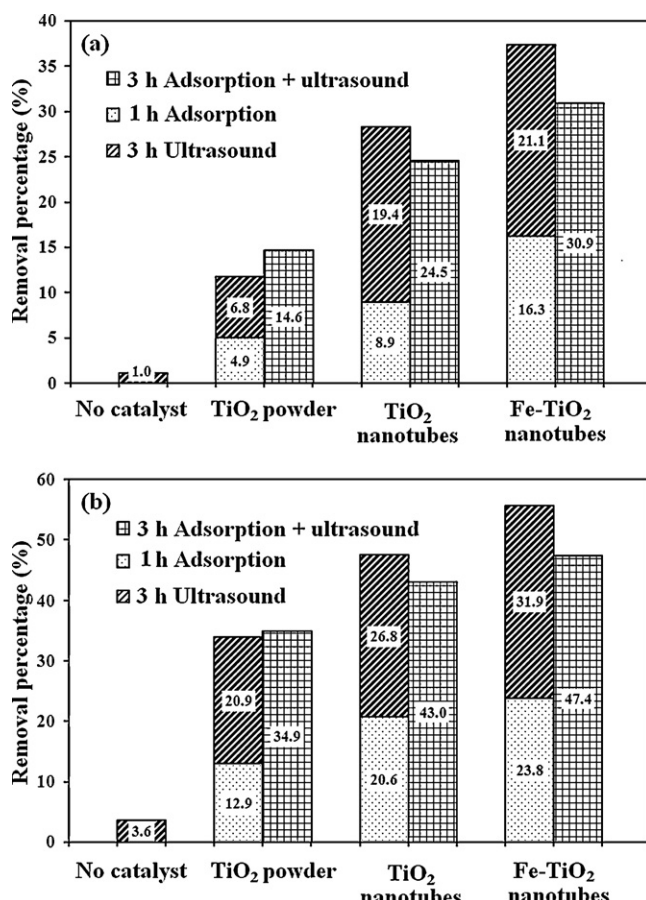


Fig. 6. Removals of (a) COD and (b) color without and with different catalysts under ultrasonic irradiation (Solution pH=3, catalyst dosage=6 g/L, temperature=30 °C±2, reaction time=3 h).

3.2. Sonocatalytic degradation of textile effluent

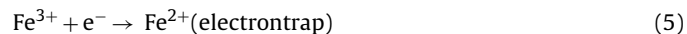
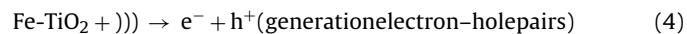
Two types of reaction system were performed to distinguish the effect of adsorption and sonocatalytic activities of various catalysts on the removal efficiency of real textile wastewater. The first reaction solution was carried out with an adsorption process for 1 h in order to ensure the establishment of an adsorption-desorption equilibrium of organics dyes on the catalyst surface before subjected to 3 h of ultrasonic irradiation as described in Section 2.4. Another set of heterogeneous reaction system was exposed directly to 3 h of ultrasonic irradiation. For convenience, the former and latter reaction systems are denoted as A–S and A+S, respectively. It was noted that there was no significant removal in the A+S system when the experiment was extended to 4 h under ultrasonic wave.

Fig. 6 shows a comparison removal efficiency of real textile wastewater in two types of reaction systems with the presence of various catalysts. The degradation in the A+S system (COD and color removal were 14.6% and 34.9%, respectively) of real textile wastewater in the presence of TiO₂ powder was unexpectedly slightly higher than in the A–S system (COD and color removal were 11.7% and 33.8%, respectively). This result was consistent with the photocatalytic reaction reported by Shon et al. [28]. In their study, the simultaneous adsorption and photocatalysis led to a superior dissolved organic removal compared to adsorption followed by photocatalysis. Meanwhile, the saturated sorbates on the small surface area of TiO₂ powder would hinder the sonocatalytic degradation [4].

In contrast, real textile wastewater in the presence of TiO₂ nanotubes showed higher removal efficiency in the A–S system than

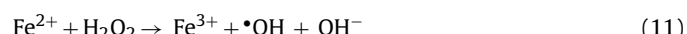
A+S system. The different trend observed in two reaction systems could be ascribed to the extent of adsorption of dye molecules due to the different surface area and surface charge of catalysts [29]. Saoudi and Hamdaoui [30] and Chakma and Moholkar [31] concluded that the acoustic or shock waves generated by ultrasound could promote the desorption of organic pollutants from activated carbon. Hence, the dye adsorption process on heterogeneous catalyst might be negated by desorption process under the ultrasonic. It is believed that the oxidative removal ability is directly proportional to the adsorption capability [4]. The shorter contact time between dye molecules and catalyst surface in the A+S system led to lower reaction of adsorbed dyes with •OH radicals. Besides, TiO₂ nanotubes had higher surface area to adsorb more dye molecules. In short, the significant amount of dye molecules adsorbed on the surface of catalyst results in enhancement of sonocatalytic degradation. The degradation of real textile wastewater in the presence of TiO₂ nanotubes in the A–S system was used in the following sections to demonstrate the process behaviors.

Fe-doped TiO₂ nanotubes exhibited excellent absorbability and sonocatalytic activity for real textile effluent, which are much higher than that of TiO₂ powder and TiO₂ nanotubes. Many researchers [10,32] reported that flash light/energy dissipation during acoustic cavitation which equals or exceeds the band gap energy of the TiO₂-based sonocatalyst is able to excite the sonocatalyst. A valence band electron could be promoted to the conduction band, leaving behind holes at the valence band (Eq. (4)). It is generally accepted that the Fe³⁺ can act as shallow trapping site for charge carrier (electron (e⁻) or h⁺) as shown in Eq. (5)–(6) [23,33]. It has been reported that the Fe³⁺/Fe²⁺ energy level is just below the conduction band of Ti³⁺/Ti⁴⁺, while the Fe³⁺/Fe⁴⁺ energy level is slightly above the valence band of TiO₂ [33]. This could favor the separation of h⁺ and e⁻ to accelerate sonocatalytic reactions for the degradation of organic dyes. The mean lifetime of an electron–hole pair is about 30 ns and this could be extended to minutes after doping with Fe³⁺ [34]. The unstable Fe²⁺ and Fe⁴⁺ as compared to Fe³⁺ had a tendency for the transfer of the trapped charges from Fe²⁺ and Fe⁴⁺ ions to Fe³⁺ as shown in reactions (7) and (8) [35]. Besides, higher surface area, good anatase crystallinity and lower energy band gap may be important factors in determining fast oxidation reactions.



where)) denotes ultrasonic irradiation.

In addition, water molecule would be degraded under acoustic cavitation to release active •OH and •H (Eq. (9)). The extent of Fe leaching for the Fe-doped TiO₂ nanotubes was about 8.89% (0.0825 ppm) for the process performed at pH 3. The amount of Fe ions were found to be <0.2 ppm, which is below the permissible level [36]. However, the reaction between the leached amount of Fe ions in the solution under ultrasonic irradiation and hydrogen peroxide which was generated from Eq. (10)–(11) should not be ruled out [17].



As shown in Fig. 6, 1 h of adsorption was able to compete with the case of 3 h of ultrasonic degradation in some cases. However,

it should be noted that adsorption process is merely transforming the dye molecules from its aqueous phase to a solid phase to generate a secondary pollutant. The ultrasonic degradation through advanced oxidation process could offer a more effective treatment to achieve complete mineralization of dye pollutants. Similar to photocatalytic process [28,37], the requirement of these processes is to restrain the recombination of electron–hole pairs produced from excited TiO_2 , and further generate active species such as h^+ and $\cdot\text{OH}$. The main difference between photocatalytic and sonocatalytic processes is the type of energy source used to initiate the oxidation reactions [13].

The generated $\cdot\text{OH}$ is a powerful oxidizing agent which is able to attack the organic dye at or near the surface of TiO_2 . Besides, the h^+ can directly oxidize organic dyes adsorbed on the surface of catalyst or degrade them indirectly through $\cdot\text{OH}$ generated by the reaction between h^+ and water molecules [15]. Meanwhile, the amount of adsorbed molecular oxygen on the catalyst surface was reduced by e^- to yield a host of reactive oxygen species [15,37]. Recently, Wang's group [32,37] made attempts for the detection of such reactive oxygen species that were generated when TiO_2 powder was irradiated with ultrasound. However, accurate measurement of these species was difficult due to the short life span of the active species. Therefore, no measurement of these species test was conducted in this study as the reliability of the measurement could not be confirmed. Besides, the scope of this study was only dedicated to the effect of operating parameters for adsorption–sonocatalytic degradation of real textile wastewater.

3.3. Influence of reaction conditions on the sonocatalytic degradation process

3.3.1. Effect of solution pH

pH value is one of the most important parameters that should be taken into consideration to determine the suitability of the discharged effluent for subsequent wastewater treatment stages. Fig. 7 shows that the degradation of real textile wastewater was significantly influenced by the solution pH and the highest degradation rate was achieved at pH 3. Solution pH would affect both chemical form of reactants and surface binding-sites of the catalysts. The surface charge of the Fe-doped TiO_2 nanotubes as a function of solution pH has been shown previously using the zeta potential diagram (Fig. 4). Therefore, attractive forces between the anionic dye molecules and positively charged catalyst surface would favour adsorption at pH below pH_{Zpc} . The highest adsorption process based on COD and color removals were found to occur in acidic solution (Fig. 7). This indicated that real textile wastewater consisted mostly of anionic dyes rather than cationic dyes.

Similarly, when the solution pH is lower than acid-base dissociation constant (pK_a) of the reactant, the organic dye compounds mainly exist as neutral molecules in water [7]. The effect of protonation could enrich the hydrophobic character and accumulate in the interface of cavitation bubbles [1]. This was more readily subjected for the $\cdot\text{OH}$ attack and enhanced its reactivity under ultrasound treatment at pH 3. It has been reported that stable $\cdot\text{OH}$ will be produced to exhibit high oxidizing potential at pH 2–4 [38].

Meanwhile, organic dyes exist in the ionized states at pH greater than pK_a of the reactant. Ionic form of organic dye could enhance the hydrophilicity and solubility in water [6]. This enables the sonocatalytic reactions to be carried out in the bulk solution which has a lower concentration of $\cdot\text{OH}$ as compared to the interface of cavitation bubbles. Ghodbane and Hamdaoui [6] reported that only 10% of $\cdot\text{OH}$ production could reach the bulk solution. The oxidation potential of $\cdot\text{OH}$ decreased and higher number of $\cdot\text{OH}$ species was able to recombine to form H_2O_2 at pH 5 to pH 9 [2,6]. Besides, Fe^{3+} would precipitate in the form of hydroxide, which inhibited the regeneration of ferrous ions and reduced the

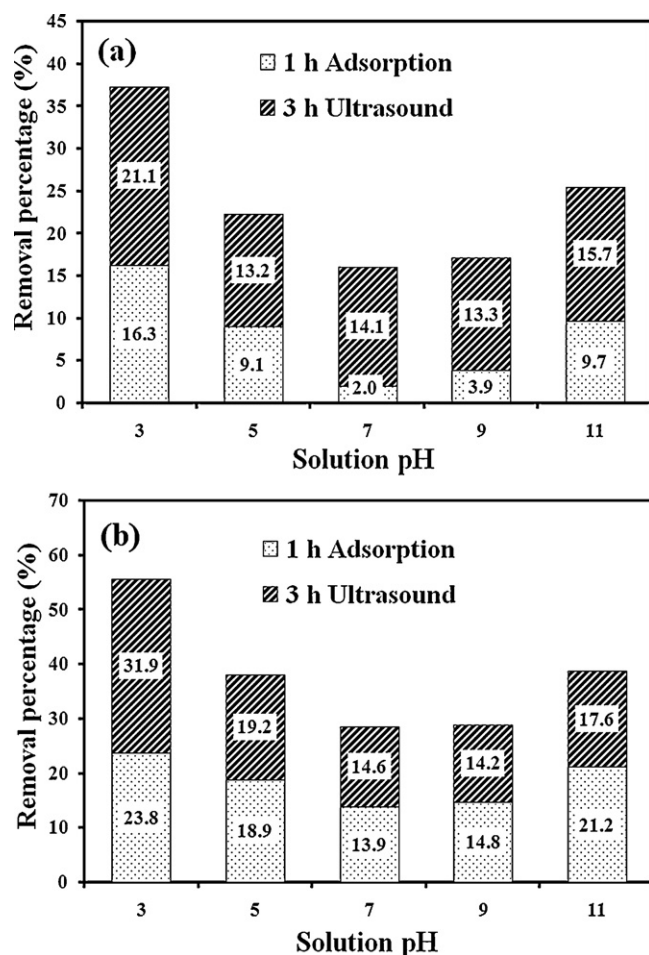


Fig. 7. Effect of solution pH on (a) COD and (b) color removals (Catalyst dosage = 6 g/L, temperature = $30^\circ\text{C} \pm 2$, reaction time = 3 h).

degradation rate [2]. Considering all these combination effects, the degradation experienced a decrease at pH 5 to pH 9. On the other hand, the enhancement of degradation rate at pH 11 might be caused by the consumption of OH^- ions by h^+ to yield $\cdot\text{OH}$ species [39]. The increase in the concentration of $\cdot\text{OH}$ could increase the degradation rate of the wastewater.

3.3.2. Effect of catalyst dosage

The sonocatalytic degradation of real textile wastewater in the presence of variable amounts of Fe-doped TiO_2 nanotubes for 3 h is shown in Fig. 8. It can be observed that the combination of catalyst and ultrasonic irradiation played a significant role to enhance the degradation efficiency. The optimum amount of catalyst (6 g/L) was needed to reach the highest degradation efficiency of about 37.4% COD and 55.7% color removal. Heterogeneous catalyst may provide additional nuclei for cavitation bubble formation [17], which would release more active species that could attack organic pollutants. It has been reported that ultrasonic waves have the potential to create microturbulence of cavitation bubbles near the surface of solid particles that could reduce the mass transfer in the boundary layer [30]. Therefore, the rate of mass transfer near the catalyst surface was increased leading to the enhancement in the heterogeneous reactions.

It is interesting to note that the sonocatalytic degradation decreased greatly even at higher adsorption due to higher amount of catalyst. Ultrasonic irradiation is expected to alleviate the drawbacks commonly demonstrated by photocatalytic reaction systems such as blockage of catalyst active sites, agglomeration or

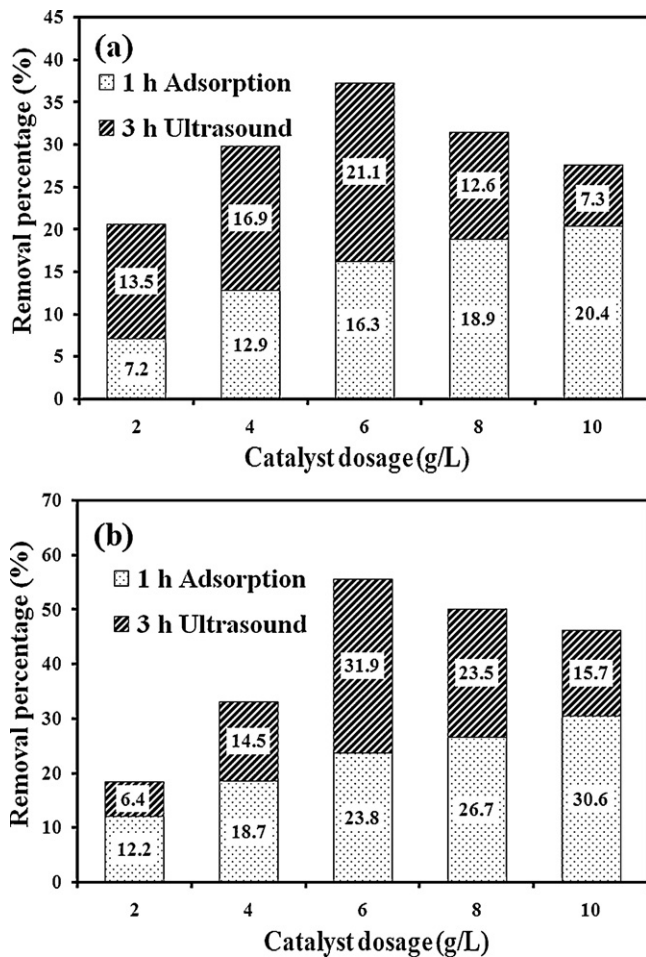


Fig. 8. Effect of catalyst dosage on (a) COD and (b) color removals (Solution pH = 3, temperature = 30 °C ± 2, reaction time = 3 h).

aggregation of the catalyst particles [40]. However, excessive dosage of catalyst can possibly block the transmission of ultrasound waves and energy near to the catalyst surface. The flash light screening and sound attenuation created adverse effect on the cavitation activity [8]. Besides, the diffusion rate of dye molecules during adsorption and desorption of partial oxidation products from the catalyst surface to bulk solution might be restricted.

Thus, adding a proper amount of catalyst for advisable adsorption process is useful to enhance the sonocatalytic degradation efficiency. It was noted that slightly higher amount of catalyst in treated real textile wastewater was reported in this study as compared to other studies for the removal of lab-prepared specific dye solution [8,17]. Optimum catalyst dosage was dependent on initial solute concentration as reported in our previous report [41]. The increase in catalyst dosage would increase the total active surface area and availability of more active sites on catalyst surface for dye molecules to be adsorbed and oxidized by ultrasound adequately.

3.3.3. Effect of H_2O_2 dosage

Fig. 9 shows the sonocatalytic degradation of real textile wastewater in the Fe-doped TiO_2 nanotubes with different dosages of H_2O_2 at pH 3. The addition of H_2O_2 could reduce the surface tension of the liquid to lower the cavitation threshold [1]. This would facilitate the generation of cavitation bubbles to consequently increase production rate of additional free reactive radicals during decomposition of H_2O_2 . Thus, the degradation rate increased with increasing concentration of H_2O_2 . The optimum dosage of H_2O_2 was about 40 mM. It has been reported that the optimum dosage of

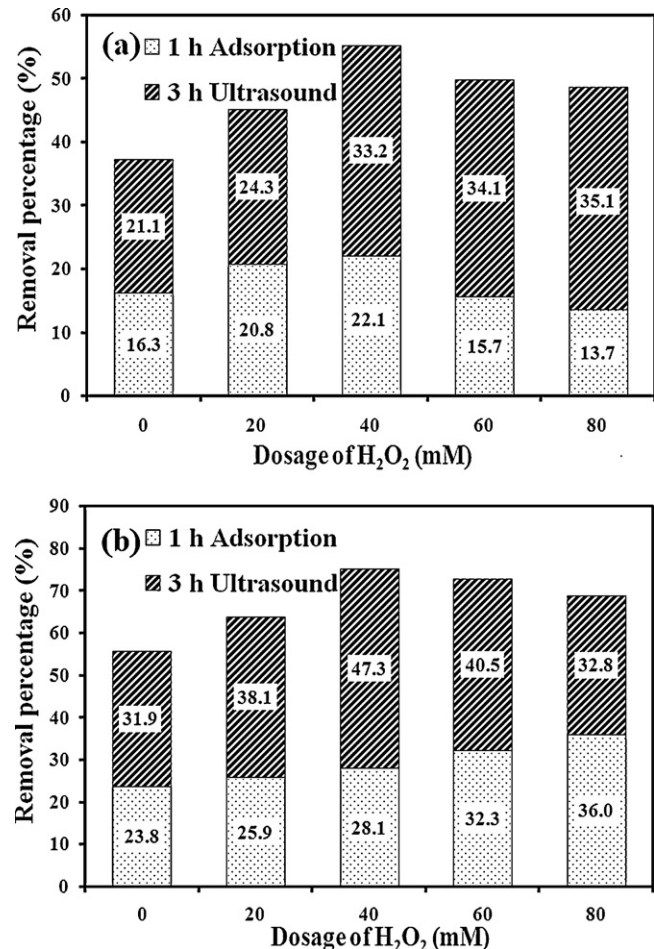


Fig. 9. Effect of H_2O_2 dosage on (a) COD and (b) color removals (Solution pH = 3, catalyst dosage = 6 g/L, temperature = 30 °C ± 2, reaction time = 3 h).

H_2O_2 was depended on initial dye concentration [42]. In addition, the leached Fe species could catalyze fenton-like and fenton reactions as discussed earlier (Eq. (10)–(11)) to increase the production of $\cdot OH$ which were capable to enhance the mineralization process.

Further increase in H_2O_2 addition after the optimum level resulted in a decrease in the degradation rate. High concentrated H_2O_2 solutions could undergo scavenging effects which is a self quenching process of $\cdot OH$ to form hydroperoxyl radicals ($\cdot OOH$) according to the following reaction (Eq. (12)) [2]. It has been reported that the oxidation potential of $\cdot OOH$ is much lower than that of $\cdot OH$ [43], leading to negligible increment in the dye degradation.



In order to evaluate the contribution of fenton-like process, homogeneous catalyzed reaction with the presence of equal amount of Fe^{3+} in Fe-doped TiO_2 nanotubes in real textile wastewater was carried out under optimum conditions. The amount of Fe^{3+} dissolved in real textile wastewater in the homogenous run was higher than the amount of Fe species leached from the Fe-doped TiO_2 nanotubes. The final COD and color removal were about 13.5% and 27.4%, respectively in the A – S system. This indicated that the catalytic reaction was mainly due to the presence of Fe in the heterogeneous catalyst rather than the trace amount of leached Fe ions.

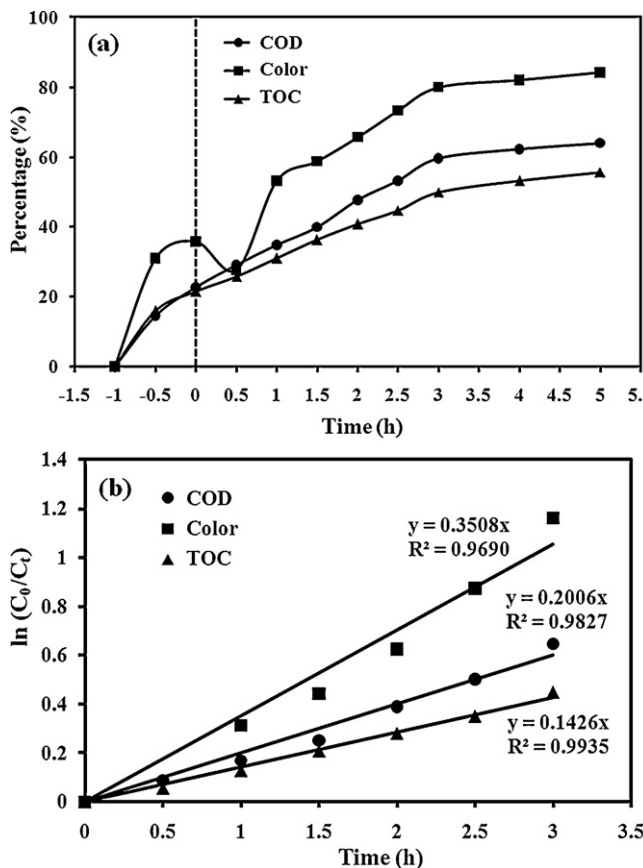


Fig. 10. (a) Effect of adsorption and ultrasonic irradiation on the removals of COD, color and TOC and, (b) kinetic plots for removal of COD, color and TOC (Solution pH = 3, catalyst dosage = 6 g/L, H_2O_2 dosage = 40 mM, aeration, temperature = $30^\circ C \pm 2$).

3.4. Effect of adsorption and ultrasonic irradiation time

The adsorption–sonocatalytic degradation of real textile wastewater in Fe-doped TiO_2 nanotubes in terms of TOC, COD and color along with the increase of ultrasonic irradiation time are shown in Fig. 10(a). After 5 h, the degradation efficiency in terms of TOC, COD and color reached 55.9%, 63.9% and 84.1%, respectively. The degradations in TOC, COD and color were much faster during the first 3 h of sonocatalytic degradation and it can be stated that 3 h of ultrasonic irradiation is sufficient for degradation of real textile wastewater. This is due to the fact that the intermediate products such as aliphatic acids and aldehydes are difficult to further oxidize than their parent compounds (dye molecules), and complete oxidation may proceed at a much slower reaction rate [3]. The degree of carbon mineralization (TOC removal) was slightly lower than COD removal efficiency under the same tested operating conditions due to the generation of carboxylic acids and aldehydes as final products rather than carbon dioxide [3].

The mechanism of heterogeneous catalysis adsorption–sonocatalytic reactions may involve (i) mass transfer from bulk solution to catalyst surface, diffusion within porous particles and adsorption of organic dye molecules on catalyst surface, (ii) surface oxidation reaction between adsorbed dye molecules and $\cdot OH$ or h^+ [15], and then the products of partial oxidation may desorb from the catalyst surface. The free reactive radicals could then react with adsorbed dye molecules or diffuse away from the catalyst surface to react with dye molecules in the bulk solution. The partitioning of reaction processes occurring at or near the catalyst surface is strongly influenced by the strength of adsorption

capacity [44]. In this case, adsorption process played an important role in sonocatalytic process as it showed significant color removal (34.9%) before being subjected to ultrasonic irradiation. This result suggested that the acceleration of sonocatalytic reaction mainly occurred in the adsorbed phase at the surface of Fe-doped TiO_2 nanotubes rather than in the bulk solution.

It was interesting that unexpected increment of the color intensity at the initial stage of sonocatalytic degradation (within 30 min) was observed. This result revealed that desorption of dye molecules from Fe-doped TiO_2 nanotubes occurred simultaneously during heterogeneous sonocatalytic degradation, leading to an increase in the color initially. Shon et al. [28] also observed a similar initial increase of dissolved oxygen concentration (reverse reaction) during photocatalysis and aimed for its elimination. Acoustic cavitation could produce high-pressure shockwaves, high-speed microjets, microstreaming and microturbulence that impinged incessantly on the catalyst surface [30,31]. These phenomena will lead to the partial desorption of adsorbed molecules into the solution to be more effectively oxidized by $\cdot OH$. However, this reverse reaction was deemed transient and was observed only at the beginning of sonocatalysis. Thus, it contributed only to a small impact on the initial removal efficiency because desorption of dye molecules from catalyst surface was also degraded into smaller organic compounds as the sonocatalysis reaction proceeded.

Furthermore, it should be noted that the shock waves produced during bubbles collapsed had the potential of creating microscopic turbulence within interfacial film surrounding nearby solid particles [30]. This phenomenon might cause TiO_2 nanotubes to be destroyed and crushed to form smaller tubes or fragments. However, this catalyst did not suffer the drawback of difficult separation after the slurry-type catalytic reaction. Our recent results proved the stability of Fe- TiO_2 nanotubes after being reused for 4 cycles [19].

The sonocatalytic degradation reaction within the first 3 h obeyed the apparent first-order kinetic ($\ln C_t/C_0 = -k_{app}t$) where C_0 and C_t are the concentration of organic dye at reaction time = 0 and t , respectively, t is the irradiation time and k_{app} is denotes as the apparent first-order rate constant. By plotting $\ln(C_0/C_t)$ as a function of ultrasonic irradiation time (t) as shown in Fig. 10(b), the k_{app} were obtained from the slope of the best fit lines. The reaction rate constant for color, COD and TOC removal are 0.3058, 0.2006 and 0.1426 h^{-1} , respectively. From the practical application point of view in textile industry as indicated in TOC and COD removal, sonocatalytic degradation showed the potential to be used as pre-treatment technology. Acoustic and hydrodynamic cavitation as pre-treatment could reduce the toxicity and enhance the biodegradability of un-treated wastewater effluent [5,45]. Sangve and Pandit [5] found that the extent of degradation under acoustic cavitation was almost double as compared to un-treated wastewater before subjected to conventional biological process. Meanwhile, Padoley et al. [45] reported the efficiency of the post-conventional biological process was increased by almost 6 fold in terms of COD removal and biogas formation.

4. Conclusions

This study showed that Fe-doped TiO_2 nanotubes catalysts could be obtained successfully using a sol-gel followed hydrothermal synthesis processes. The incorporation of Fe^{3+} dopant into the TiO_2 nanotubes could maintain excellent tubular morphologies and resulted in a material with high specific surface area and low energy band gap. Fe-doped TiO_2 nanotubes catalysts showed much higher catalytic activity for the degradation of real textile wastewater in the A–S system as compared to the A+S system. Thus, adequate adsorption of dye molecules would increase the efficiency in the oxidative degradation process.

The optimum conditions for the highest degradation efficiency were achieved at 6 g/L of Fe-doped TiO₂ nanotubes, 40 mM of H₂O₂, aerated solution, ultrasonic frequency of 35 kHz and output power of 50 W. Under these conditions, pre-adsorption on TiO₂ nanotubes was found to improve sonocatalytic degradation and the latter process could be considered as a surface-catalyzed reaction which took place on the dye-adsorbed sites on the catalyst surface. The apparent first-order reaction rate constants for color, COD and TOC removal were 0.3058, 0.2006 and 0.1426 h⁻¹, respectively. Thus, the combination of adsorption and heterogeneous sonocatalysis performed very well in treating the real dye-containing wastewater to satisfy the growing environmental demands.

Acknowledgements

The contribution of Prof. Subhash Bhatia in shaping up catalysis research capability at School of Chemical Engineering, Universiti Sains Malaysia needs special acknowledgement. Financial support provided by the Research University (RU) grant, a Post Graduate Research Grant Scheme and A Fellowship from Universiti Sains Malaysia are also gratefully acknowledged.

References

- [1] S. Merouani, O. Hamdaoui, F. Saoudi, M. Chiha, Chemical Engineering Journal 158 (3) (2010) 550–557.
- [2] J.-H. Sun, S.-P. Sun, J.-Y. Sun, R.-X. Sun, L.-P. Qiao, H.-Q. Guo, M.-H. Fan, Ultrasonics Sonochemistry 14 (6) (2007) 761–766.
- [3] S. Cortez, P. Teixeira, R. Oliveira, M. Mota, Journal of Hazardous Materials 182 (1–3) (2010) 730–734.
- [4] K. Hu, X. Xiao, X. Cao, R. Hao, X. Zuo, X. Zhang, J. Nan, Journal of Hazardous Materials 192 (2) (2011) 514–520.
- [5] P.C. Sangave, A.B. Pandit, Ultrasonics Sonochemistry 11 (3–4) (2004) 197–203.
- [6] H. Ghodbane, O. Hamdaoui, Ultrasonics Sonochemistry 16 (5) (2009) 593–598.
- [7] J. Liang, S. Komarov, N. Hayashi, E. Kasai, Ultrasonics Sonochemistry 14 (2) (2007) 201–207.
- [8] L. Yin, J. Gao, J. Wang, B. Wang, R. Jiang, K. Li, Y. Li, X. Zhang, Separation and Purification Technology 81 (1) (2011) 94–100.
- [9] S. Zhang, Ultrasonics Sonochemistry 19 (4) (2012) 767–771.
- [10] Z.D. Meng, W.C. Oh, Ultrasonics Sonochemistry 18 (3) (2011) 757–764.
- [11] J. Wang, Z. Jiang, Z. Zhang, Y. Xie, Y. Lv, J. Li, Y. Deng, X. Zhang, Separation and Purification Technology 67 (1) (2009) 38–43.
- [12] L. Zhang, R. Liu, H. Yang, Physica E (Low-Dimensional Systems and Nanostructures) 44 (7–8) (2012) 1592–1597.
- [13] Y.L. Pang, A.Z. Abdullah, S. Bhatia, Applied Catalysis B 100 (1–2) (2010) 393–402.
- [14] K.-Z. Zhang, B.-Z. Lin, Y.-L. Chen, B.-H. Xu, X.-T. Pian, J.-D. Kuang, B. Li, Journal of Colloid and Interface Science 358 (2) (2011) 360–368.
- [15] J. Wang, W. Sun, Z. Zhang, Z. Jiang, X. Wang, R. Xu, R. Li, X. Zhang, Journal of Colloid and Interface Science 320 (1) (2008) 202–209.
- [16] J. Wang, Y. Lv, Z. Zhang, Y. Deng, L. Zhang, B. Liu, R. Xu, X. Zhang, Journal of Hazardous Materials 170 (1) (2009) 398–404.
- [17] N.A. Jamalluddin, A.Z. Abdullah, Ultrasonics Sonochemistry 18 (2) (2011) 669–678.
- [18] C.-C. Tsai, H. Teng, Applied Surface Science 254 (15) (2008) 4912–4918.
- [19] Y.L. Pang, A.Z. Abdullah, Journal of Hazardous Materials 235–236 (0) (2012) 326–335.
- [20] F. Lin, D. Jiang, Y. Lin, X. Ma, Physica B 403 (13–16) (2008) 2193–2196.
- [21] HACH, (Hach Company) DR/890 Colorimeter Procedure Manual <http://www.hach.com>, patent pending (accessed on 12.09.12).
- [22] D.V. Bavykin, M. Caravetta, A.N. Kulak, F.C. Walsh, Chemistry of Materials 22 (8) (2010) 2458–2465.
- [23] Y. Yalcin, M. Kilic, Z. Cinar, Applied Catalysis B 99 (3–4) (2010) 469–477.
- [24] E. Morgado Jr., M.A.S. De Abreu, G.T. Moura, B.A. Marinkovic, P.M. Jardim, A.S. Araujo, Chemistry of Materials 19 (4) (2007) 665–676.
- [25] O.C.C. Wang, K.W. Wang, T.P. Perng, Applied Physics Letters 96, 143102 (2010); <http://dx.doi.org/10.1063/1.3373607> (3 pages).
- [26] M. Sahu, K. Suttiponparnit, S. Suvachittanont, T. Charinpanitkul, P. Biswas, Chemical Engineering Science 66 (15) (2011) 3482–3490.
- [27] N. Bao, Z. Wei, Z. Ma, F. Liu, G. Yin, Journal of Hazardous Materials 174 (1–3) (2010) 129–136.
- [28] H.K. Shon, S. Vigneswaran, H.H. Ngo, J.H. Kim, Water Research 39 (12) (2005) 2549–2558.
- [29] L. Xiong, W. Sun, Y. Yang, C. Chen, J. Ni, Journal of Colloid and Interface Science 356 (1) (2011) 211–216.
- [30] F. Saoudi, O. Hamdaoui, Microporous Mesoporous Materials 141 (1–3) (2011) 69–76.
- [31] S. Chakma, V.S. Moholkar, Chemical Engineering Journal 175 (1) (2011) 356–367.
- [32] J. Wang, Y. Guo, B. Liu, X. Jin, L. Liu, R. Xu, Y. Kong, B. Wang, Ultrasonics Sonochemistry 18 (1) (2011) 177–183.
- [33] J. Li, J. Xu, W.-L. Dai, H. Li, K. Fan, Applied Catalysis B 85 (3–4) (2009) 162–170.
- [34] O. Carp, C.L. Huisman, A. Reller, Progress in Solid State Chemistry 32 (1–2) (2004) 33–177.
- [35] Z. Li, W. Shen, W. He, X. Zu, Journal of Hazardous Materials 155 (3) (2008) 590–594.
- [36] N. Panda, H. Sahoo, S. Mohapatra, Journal of Hazardous Materials 185 (1) (2011) 359–365.
- [37] Y. Guo, C. Cheng, J. Wang, Z. Wang, X. Jin, K. Li, P. Kang, J. Gao, Journal of Hazardous Materials 192 (2) (2011) 786–793.
- [38] S. Mohajeri, H.A. Aziz, M.H. Isa, M.A. Zahed, M.N. Adlan, Journal of Hazardous Materials 176 (1–3) (2010) 749–758.
- [39] Y.-N. Liu, D. Jin, X.-P. Lu, P.-F. Han, Ultrasonics Sonochemistry 15 (5) (2008) 755–760.
- [40] Y.G. Adewu-Yi, Environmental Science and Technology 39 (22) (2005) 8557–8570.
- [41] Y.L. Pang, A.Z. Abdullah, S. Bhatia, Chemical Engineering Journal 166 (3) (2011) 873–880.
- [42] S. Hajji, B. Benstaali, N. Al-Bastaki, Chemical Engineering Journal 168 (1) (2011) 134–139.
- [43] V. Dulman, S.M. Cucu-Man, R.I. Olariu, R. Buhaceanu, M. Dumitras, I. Bunia, Dyes and Pigments 95 (1) (2012) 79–88.
- [44] U. Khan, N. Benabderrazik, A.J. Bourdelais, D.G. Baden, K. Rein, P.R. Gardinali, L. Arroyo, K.E. O'Shea, Toxicology 55 (5) (2010) 1008–1016.
- [45] K.V. Padole, V.K. Saharan, S.N. Mudliar, R.A. Pandey, A.B. Pandit, Journal of Hazardous Materials 219–220 (0) (2012) 69–74.